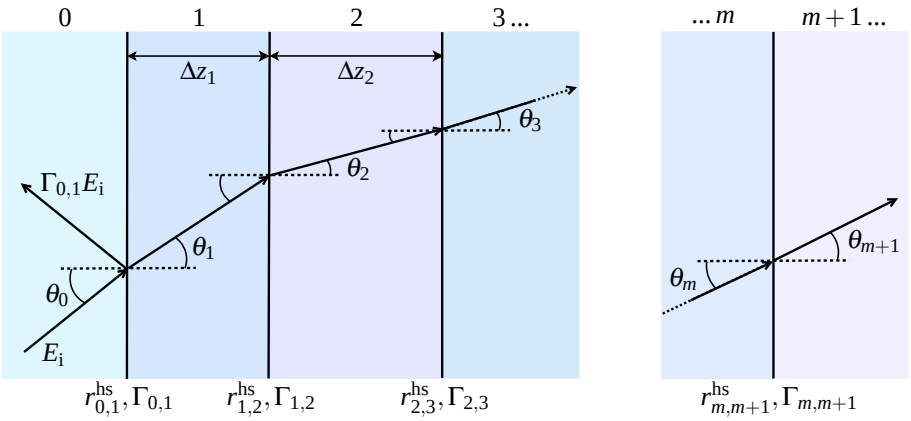

Fig. 2. Reflectivity from an N-layered system of slabs. Only the penetrating beam is shown after the initial interface. The compound reflectivity at the initial interface, $\Gamma_{0,1}$, has a component from reflectivity at each subsequent interface according to Eq. (5).

3.4. The coherent scattering model (CSM) and the effective optical properties of a colloidal system

As outlined in [26], taking into account the Mie scattering of particles, it is possible to determine an effective electric permittivity ε^{eff} and magnetic permeability μ^{eff} for a dilute system of random spheres that describe the propagation of the coherent beam. These derived optical coefficients are not continuous functions of space, but depend on the angle of light with respect to the z-axis and the light's polarisation. When ε^{eff} and μ^{eff} are substituted into Eq. (2), employing Eq. (3), an expression for the reflectivity of a half space of dilute random spheres is established. We note that the half space reflectivity is derived from wave scattering theory and does not rely on the interpretation of the system as an effective medium. The effective optical coefficients depend on the Mie scattering amplitude functions $S_j\left(\theta, x, m_{\text{p}}/m_{\text{m}}\right)$ as defined in [35], where $j = 1$ is employed for $\perp$ polarised light and $j = 2$ for $\parallel$ polarised light. The Mie scattering amplitude functions depend on the ratio of the complex refractive index of the particles to the complex refractive index of the surrounding medium, $m_{\text{p}}/m_{\text{m}}$. In the retrievals presented in this paper, it is assumed that the particles are non-absorbing (the uncertainty associated with retrievals of n_{p} arising from assuming $k_{\text{p}} = 0$ is shown to be negligible in section 4) and the suspension medium is non-absorbing, so that $m_{\text{p}}/m_{\text{m}} = n_{\text{p}}/n_{\text{m}}$. The Mie scattering amplitude functions also depend on the size paramter of particles: $x = 2\pi a/\lambda_{\text{m}}$, where $\lambda_{\text{m}} = n_{\text{m}}/\lambda_0$ is the wavelength of light in the suspension medium and λ_0 is the vacuum laser wavelength. The effective optical properties for $\perp$ polarised incident light are:

$$\frac{\mu_{\perp}^{\text{eff}}}{\mu_0} = 1 + i\gamma \frac{S_{-}^{(1)}(\theta_{\text{i}})}{\cos^2\theta_{\text{i}}}, \tag{7}$$

$$\frac{\varepsilon_{\perp}^{\text{eff}}}{\varepsilon_0} = 1 + i\gamma \left[2S_{+}^{(1)}(\theta_{\text{i}}) - S_{-}^{(1)}(\theta_{\text{i}})\tan^2\theta_{\text{i}}\right], \tag{8}$$

where

$$S_{+}^{(j)}(\theta_i) = \frac{1}{2}\left[S(0) + S_j(\pi - 2\theta_{\text{i}})\right], \tag{9}$$

$$S_{-}^{(j)}(\theta_{\text{i}}) = S(\theta_{\text{i}}) - S_j(\pi - 2\theta_{\text{i}}). \tag{10}$$

#247358 Received 5 Aug 2015; revised 27 Oct 2015; accepted 4 Nov 2015; published 25 Jan 2016

Here $\gamma = 3f/2x^3$, and f is the volume filling fraction occupied by the particles.

For $\parallel$ polarised incident light, the corresponding expressions are:

$$\frac{\varepsilon_{\parallel}^{\text{eff}}}{\varepsilon_0} = 1 + i\gamma \frac{S_{-}^{(2)}(\theta_{\text{i}})}{\cos^2\theta_{\text{i}}}, \tag{11}$$

$$\frac{\mu_{\parallel}^{\text{eff}}}{\mu_0} = 1 + i\gamma \left[2S_{+}^{(2)}(\theta_{\text{i}}) - S_{-}^{(2)}(\theta_{\text{i}}) \tan^2\theta_{\text{i}} \right]. \tag{12}$$

Substitution of Eqs. (7) and (8) for $\perp$ polarised light or Eqs. (11) and (12) for $\parallel$ polarised light into Eq. (2) yields Eq. (13) an expression for the reflection coefficient for a half space of random particles r_{hs}, as depicted in Fig. 3(a). The centres of the particles lie in the region $z > 0$ but due to the finite size of the particles some protrude into the region $z < 0$. The expression for the half space reflection coefficient is:

$$r_{\text{hs}}^{\text{eff}}(\theta_{\text{i}}) = \frac{\gamma S_j(\pi - 2\theta_{\text{i}})/\cos\theta_{\text{i}}}{i\left(\cos\theta_{\text{i}} + \left\{ \cos^2\theta_{\text{i}} + 2i\gamma S(0) - \frac{\gamma^2}{\cos^2\theta_{\text{i}}} \left[S(0)^2 - S_j(\pi - 2\theta_{\text{i}})^2 \right] \right\}^{1/2} \right) - \frac{\gamma S(0)}{\cos\theta_{\text{i}}}} \tag{13}$$

where $j = 1$ for $\perp$ polarised incident light and $j = 2$ for $\parallel$ polarised light.

The z-component of the wavevector of the coherent beam in the scatterting medium $k_{\text{z}}^{\text{eff}}$ is given by:

$$k_{\text{z}}^{\text{eff}} = \sqrt{(k_{\text{m}}^z)^2 - 2i\chi S(0) k_{\text{m}}^z/\cos\theta_{\text{i}} + (\chi^2/\cos^2\theta_{\text{i}}) \left[S_j(\pi - 2\theta_{\text{i}})^2 - S(0)^2 \right]} \tag{14}$$

where $\chi = -3f/2a^3k_{\text{m}}^2$ and a is the particle radius. We note that Eqs. (13) and (14) are derived from a wave-scattering approach, and do not rely on the interpretation of the system as an effective medium [26, 27].

Now consider the case of an interface (located at $z = 0$) between an incident medium ($z < 0$) and a turbid medium ($z > 0$) containing randomly located spheres with a dilute concentration, as depicted in Fig. 3(b). Given the condition that no particles in the turbid medium may protrude into the incident medium, the centres of all particles must lie in the region $z > a$. Thus there exists an excluded slab of width $\Delta z = a$ in which the centres of particles may not lie and application of Eq. (4) yields the interface reflectivity:

$$r = \frac{r_{\text{i,m}}^{\text{Fres}} + r_{\text{hs}}^{\text{eff}}(\theta_{\text{m}}) \exp(2ik_{\text{m}}^z a)}{1 + r_{\text{i,m}}^{\text{Fres}} r_{\text{hs}}^{\text{eff}}(\theta_{\text{m}}) \exp(2ik_{\text{m}}^z a)}, \tag{15}$$

where $r_{\text{i,m}}^{\text{Fres}}$ is the Fresnel reflectivity for an interface between a homogeneous medium with refractive index n_{i} and a homogeneous medium with refractive index n_{m}.

3.5. Polydisperse systems

The expressions for the optical coefficients are easily modified to account for polydisperse particle size distributions. The amplitude scattering function $S_j(\theta, a)$, in Eqs. (7), (8), (11) and (12), is replaced by an average value integrated over the size distribution: $\int_0^\infty S_j(\theta, a)\, n(a)\, da$, where $n(a)$ is the normalised size distribution function (such that $\int_0^\infty n(a)\, da = 1$).

As outlined in [29], an additional complication arises when modelling the reflectivity at an interface between an incident medium and a turbid medium containing a random dilute system

#247358 Received 5 Aug 2015; revised 27 Oct 2015; accepted 4 Nov 2015; published 25 Jan 2016

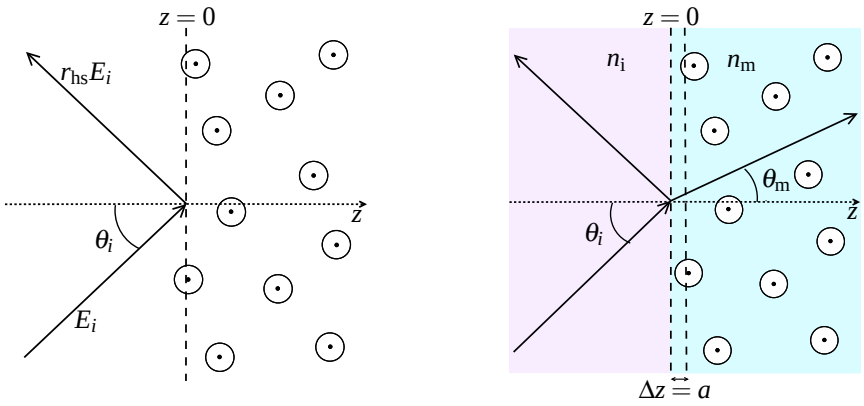

(a) Reflectivity from a half space of spheres.

(b) Reflectivity at an interface between an incident medium and a turbid medium containing randomly located spheres.

Fig. 3. Reflectivity from two systems containing random spheres.

of polydisperse particles: A particle of radius a cannot approach closer than a to the interface, resulting in the relative density of smaller particles increasing as the interface is approached. Thus the size distribution close to the interface is modified according to:

$$n(a,z) = U(z-a)\,n(a), \tag{16}$$

where $U(x)$ is a step function defined by: $U(x) = 0$ for $x < 0$, and $U(x) = 1$ for $x \geq 0$. Sufficiently far from the interface, the distribution is described by the unmodified distribution $n(a)$.

In order to model the coherent reflectivity from a polydisperse colloid, the system can be split into three parts: the incident medium at $z < 0$; a transition region inside the colloid consisting of N slabs of equal width Δz extending from $z = 0$ to $z = N\Delta z$; and finally a region with the unmodified bulk distribution $n(a)$ occupying $z > N\Delta z$. In the model approximation, within the transition region, the size distribution of particles is assumed to be constant within each slab but varies between slabs. Figure 4 demonstrates how the particle size distribution in slab m of the transition region is restricted to particles with radius $a < m\Delta z$. Such a system provides an approximation that tends to the modified distribution described by Eq. (16) as Δz becomes small and N large.

In order to determine the reflectivity from the approximate model system depicted in Fig. 4, Eqs. (7) and (8) or (11) and (12) (depending on the polarisation) must be used to establish the effective optical properties of each slab, integrating the amplitude scattering function $S_j(\theta,a)$ over the appropriately truncated particle size distribution. For slab m the appropriate replacement being: $\int_0^{m\Delta z} S_j(\theta,a)\,n(a)\,da$. In the region $z > N\Delta z$ the appropriate replacement is the integral over the entire distribution: $\int_0^{\infty} S_j(\theta,a)\,n(a)\,da$.

Once the effective optical properties of each region of the approximate model system have been established, the system reflectivity Γ_{01} can be readily calculated using successive applications of Eq. (5). In the retrievals performed on the polydisperse volcanic ash and the polydisperse sand sample, a lognormal distribution was assumed with a median radius, a_0, and a geometric standard deviation, S:

#247358 Received 5 Aug 2015; revised 27 Oct 2015; accepted 4 Nov 2015; published 25 Jan 2016

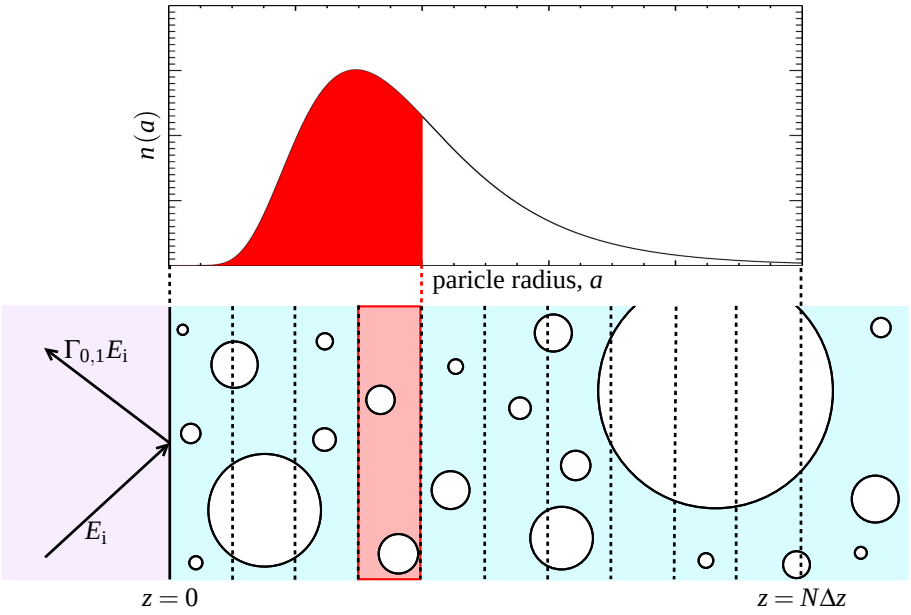

Fig. 4. Illustration of modelling the reflectivity from a polydisperse colloid, using an N-slab transition region extending from $z = 0$ to $z = N\Delta z$. The diagram illustrates how in slab m the distribution of particles is restricted to those with radius $a < m\Delta z$.

$$n(a) = \frac{1}{\sqrt{2\pi}\ln(S)\,a}\exp\left[\frac{\ln(a)-\ln(a_0)}{2\ln^2(S)}\right]. \tag{17}$$

4. Sensitivity analysis

In order to determine how measurement errors and other errors propagate through the forward model into uncertainty associated with the retrieved real refractive index n_p, a sensitivity analysis was performed for the monodisperse model and the polydisperse model.

4.1. Error propagation formalism

We follow the error analysis formalism outlined in [39]. For the general problem, the measurement vector, $\mathbf{y}$, is related to the state vector, $\mathbf{x}$, and the measurement error, $\boldsymbol{\varepsilon}$, via:

$$\mathbf{y} = \mathbf{F}(\mathbf{x},\mathbf{b}) + \boldsymbol{\varepsilon}, \tag{18}$$

where $\mathbf{F}(\mathbf{x},\mathbf{b})$ is the forward model, and $\mathbf{b}$ is the set of assumed forward model parameters. In this application, the measurement vector $\mathbf{y}$ contains the set of m detector readings recorded for the specularly reflected beam at m values of the incidence angle θ_i. The state vector $\mathbf{x}$ contains all retrieved parameters, including the real refractive index of the particles n_p. The vector $\mathbf{b}$ consists of quantities that influence the measurement and are known to some level of accuracy, but are not retrieved quantities.

After linearising about a reference state, $\mathbf{x}_0$, Eq. (18) becomes:

$$\mathbf{y} - \mathbf{F}(\mathbf{x}_0,\mathbf{b}) = \mathbf{K}(\mathbf{x}-\mathbf{x}_0) + \boldsymbol{\varepsilon}, \tag{19}$$

#247358 Received 5 Aug 2015; revised 27 Oct 2015; accepted 4 Nov 2015; published 25 Jan 2016

where $\mathbf{K}$ is the Jacobian defined by $\mathbf{K}_{ij} = \partial \mathrm{F_i}(\mathbf{x})/\partial \mathrm{x_j}$, corresponding to the partial derivative of a forward model element with respect to a state vector element. The dimensions of $\mathbf{K}$ are $m \times n$.

When a retrieval is performed on the experimental data, a best estimate of the state, $\hat{\mathbf{x}}$, is produced:

$$\hat{\mathbf{x}} = \mathbf{R}(\mathbf{y}, \mathbf{b}), \tag{20}$$

and after linearising this becomes:

$$\hat{\mathbf{x}} = \mathbf{G}\mathbf{y}, \tag{21}$$

where $\mathbf{G}$ is the gain matrix and represents the sensitivity of the retrieved state to changes in the measurement vector, $\mathbf{G} = \partial \mathbf{R}/\partial \mathbf{y}$.

A least squares retrieval weighted by measurement error was performed on experimental data to determine the best estimate of the state, $\hat{\mathbf{x}}$. The minimised function was therefore:

$$(\mathbf{y} - \mathbf{K}\mathbf{x})^{\mathrm{T}} \mathbf{S}_{\varepsilon}^{-1} (\mathbf{y} - \mathbf{K}\mathbf{x}), \tag{22}$$

where $\mathbf{S}_{\varepsilon}$ is the measurement error covariance matrix, defined by $S_{ij} = \langle \varepsilon_i \varepsilon_j \rangle$, with ε_i being the error associated with the i^{th} measurement. The gain matrix for this type of retrieval takes the form:

$$\mathbf{G} = \left(\mathbf{K}^{\mathrm{T}} \mathbf{S}_{\varepsilon}^{-1} \mathbf{K}\right) \mathbf{K}^{\mathrm{T}} \mathbf{S}_{\varepsilon}^{-1}. \tag{23}$$

The propagated uncertainty in the retrieved state, $\mathbf{S}_x$, has two contributions. The first contribution, $\mathbf{G}\mathbf{S}_{\varepsilon}\mathbf{G}^{\mathrm{T}}$, results from the application of the retrieval to the measurement error. The second contribution, $\mathbf{G}\mathbf{K}_b\mathbf{S}_b\mathbf{K}_b^{\mathrm{T}}\mathbf{G}^{\mathrm{T}}$, results from errors associated with forward model parameters, with $\mathbf{K}_b = \partial \mathbf{F}/\partial \mathbf{b}$ being the sensitivity of the forward model to forward model parameters. The combined uncertainty associated with the retrieved state is:

$$\mathbf{S}_x = \mathbf{G}\mathbf{S}_{\varepsilon}\mathbf{G}^{\mathrm{T}} + \mathbf{G}\mathbf{K}_b\mathbf{S}_b\mathbf{K}_b^{\mathrm{T}}\mathbf{G}^{\mathrm{T}}. \tag{24}$$

4.2. Modelling error

Often simplifying assumptions are made because the real physics is either not known or cannot be modelled accurately. The modelling error is given by:

$$\mathbf{G}\Delta\mathbf{f} = \mathbf{G}\left[\mathbf{f}\left(\mathbf{x}, \mathbf{b}, \mathbf{b}'\right) - \mathbf{F}(\mathbf{x}, \mathbf{b})\right], \tag{25}$$

where $\mathbf{f}$ contains the correct physics and $\mathbf{b}'$ contains additional model parameters.

4.3. Computing sensitivities

In order to evaluate the uncertainty in retrieved quantities the forward model sensitivities, $\mathbf{K}$ and $\mathbf{K}_b$, must be computed. These are simply linearisations of the forward model — Eq. (19) — and therefore vary as a function of the state vector $\mathbf{x}$.

In order to compute these sensitivities, one element of the state vector was perturbed by a fraction of 10^{-5} about a reference state, $\mathbf{x}_0$. The forward model was then applied to compute the resulting perturbed measurement vector. The sensitivity derivative could then be calculated. By repeating for each element of the state vector, consecutive columns of the Jacobian, $K_{ij}(\mathbf{x}_0) = \partial F_i(\mathbf{x}_0)/\partial x_j$, were computed.

In addition to computing the propagated uncertainties at this reference state, it is also useful to investigate how the propagated uncertainties vary with position in state space (or assumed

#247358 Received 5 Aug 2015; revised 27 Oct 2015; accepted 4 Nov 2015; published 25 Jan 2016

model parameter space). Of particular interest is how these uncertainties vary with particle refractive index, and also with particle radius. For example, in order to investigate how the propagated uncertainties vary with particle refractive index, n_p, requires recalculation of the Jacobian over the desired range of n_p, whilst keeping the remaining parameters of the reference state fixed.

4.4. Sensitivity analysis of the monodisperse model and the polystyrene latex test particle retrieval

The analysis presented here is tailored to the type of retrieval performed on the polystyrene latex test particles. The reference state $\mathbf{x}_0$ was taken as the retrieved state from the retrieval on reflectivity data from a polystyrene latex sample with a measured volume filling fraction of $f = 6.70\,\%$. In the polystyrene particle retrievals the monodisperse model was used (the particles were manufactured to be monodisperse, with a coefficient of variation in size of $\leq 3\,\%$ quoted by the manufacturer). The state vector took the form $\mathbf{x} = \left(n_p, n_m\right)$. The parameter n_m was retrieved rather than fixed at the value of the refractive index of distilled water, because the presence of the polymer dispersant in the distilled water likely affects its refractive index. The volume filling fraction, f, which had been measured with an uncertainty of $5\,\%$ was fixed at its measured value in the retrieval and thus formed an element in the vector of assumed model parameters; additional assumed model parameters were such that $\mathbf{b} = (f, a, \lambda)$.

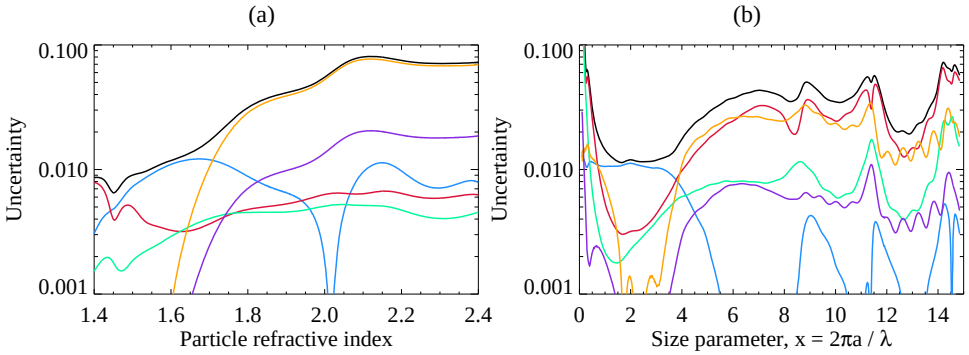

Fig. 5. The contributions to uncertainty in the retrieval of real refractive index for a monodisperse system plotted against (a) real refractive index and (b) size parameter. The contributions to the uncertainty and the combined uncertainty are shown: — volume filling fraction, — incidence angle, — laser power, — particle radius, — laser wavelength and — combined uncertainty. Uncertainty resulting from assuming non-absorbing particles was less than 0.001. The reference state was taken to be the retrieved state for a polystyrene latex sample with a measured volume filling fraction $f = 6.70\,\%$.

Figure 5 summarises the contributions to the combined uncertainty in the retrieval of real refractive index resulting from measurement uncertainties and uncertainties associated with assumed model parameters. The plots show how these error contributions vary (about the reference state) with particle refractive index and with size parameter — Figs. 5(a) and 5(b), respectively.

Table 1 sets out the contributions to propagated uncertainty at the reference state: the $f = 6.70\,\%$ retrieval result. It can be seen that the $5\,\%$ uncertainty associated with the measured volume filling fraction contributes to the largest uncertainty in the retrieved real refractive index.

The uncertainty from assuming non-absorbing particles was calculated as follows. We can then take the imaginary particle refractive index to be zero, $k_p = 0$, providing we assign a parameter error comparable to the true magnitude of k_p. Xiaoyon *et al.* [40] found k_p for polystyrene

#247358 Received 5 Aug 2015; revised 27 Oct 2015; accepted 4 Nov 2015; published 25 Jan 2016

to be less than 0.001 for $\lambda < 800$ nm. The contribution to the propagated uncertainty is then given by $\mathbf{G}\mathbf{K}_b\mathbf{S}_b\mathbf{K}_b^{\mathrm{T}}\mathbf{G}^{\mathrm{T}}$, as detailed in Eq. (24), assuming a parameter error in k_{p} of 0.001. The resulting propagated uncertainty in the retrieval of n_{p} was found to be less than 0.001 for all values of x and n_{p} investigated.

In theory there is no restriction on including the imaginary refractive index of the particles in the forward model. However, the value of the imaginary refractive index of polystyrene in the visible is very low and has very little effect on the reflectivity of the system or the retrieval of n_{p}, as demonstrated by the results of this sensitivity analysis.

Table 1. Summary of contributions to the propagated uncertainty in the retrieval of n_{p} for the retrieval using the monodisperse CSM performed on the polystyrene latex particle reflectivity data. The values shown were calculated at the retrieved state of the $f = 6.70\,\%$ scan.

Error Term, e	σ_e	Propagated uncertainty, $\left\lvert\frac{\delta n_{\mathrm{p}}}{\delta e}\right\rvert \sigma_e$.
Volume filling fraction, f	5 %	0.01070
Incidence angle, θ_{i}	0.05°	0.00331
Laser power, LP	1 %	0.00279
Particle radius, a	3 %	0.00039
Non-absorbing assumption		0.00004
Laser wavelength, λ	5 nm	0.00001
Combined uncertainty		0.01154

4.5. Sensitivity analysis for the polydisperse model and the sand and ash retrievals

This analysis is tailored to the type of retrieval performed on the sand and the volcanic ash samples. The polydisperse model, taking into account the interface region using a 50 slab system, was applied to experimental reflectivity data from these samples. A log-normal distribution was assumed, controlled by the median radius, a_0, and geometric standard deviation, S. For these retrievals the state vector took the form $\mathbf{x} = \left(n_{\mathrm{p}}, n_{\mathrm{m}}, f, a_0, S\right)$, whilst the assumed model parameter vector had the form $\mathbf{b} = (\lambda)$. The reference state $\mathbf{x}_0$ was taken to be the retrieved state for a retrieval performed on sand reflectance data in which the retrieved volume filling fraction was $f = 5.01\,\%$.

Figure 6 summarises the error contributions in the retrieval of real refractive index as a function of particle refractive index and size parameter — Fig. 6(a) and Fig. 6(b), respectively. The size parameter is defined in terms of the median radius of the log-normal distribution: $x = 2\pi a_0/\lambda$. It can be seen from Fig. 6(b) that the minimum for combined uncertainty occurs for a size parameter of approximately 1.9, which for a laser wavelength of 635 nm corresponds to a median radius of 190 nm.

Table 2 shows the values of propagated uncertainty in the retrieval of real refractive index from each of the error terms. The particular values shown in the table apply for the polydisperse retrieval, employing a 50 slab interface region, performed on a sand sample with a retrieved volume filling fraction of $f = 5.01\,\%$ (see Table 4 for the full state vector). It can seen that the largest error terms come from uncertainty in the measured incidence angles at which the reflectivity detector readings are made, and uncertainty in the laser power.

The uncertainty from assuming non-absorbing particles was calculated using a method identical to that outlined above for the monodiperse case. The imaginary particle refractive index was fixed at $k_{\mathrm{p}} = 0$ and assigned a parameter uncertainty of 0.001 — Ball *et al.* [22] measured

#247358 Received 5 Aug 2015; revised 27 Oct 2015; accepted 4 Nov 2015; published 25 Jan 2016

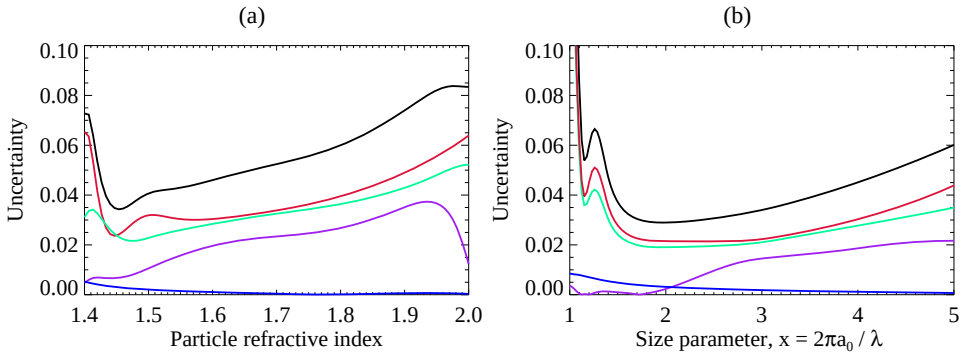

Fig. 6. The contributions to uncertainty in the retrieval of real refractive index for a polydisperse distribution taking into account the interface region using a 50 slab system: — incidence angle, — laser power, — non-spherical effects, — non-absorbing assumption and — combined uncertainty. The reference state was taken to be the retrieved state for the sand retrieval with a retrieved volume filling fraction of $f = 5.01\,\%$.

Table 2. Summary of the contributions to the propagated uncertainty in the retrieval of n_p for the polydisperse model taking into account the interface region using a 50 slab system. The reference state was taken to be the retrieved state for the sand retrieval with a retrieved volume filling fraction of $f = 5.01\,\%$.

Error Term, e	σ_e	Propagated uncertainty, $\left\lvert\frac{\delta n_\mathrm{p}}{\delta e}\right\rvert \sigma_e$.
Incidence angle, θ_i	0.05°	0.0301
Laser power, LP	1 %	0.0276
Non-spherical effects		0.0185
Non-absorbing assumption		0.0012
Laser wavelength, λ	5 nm	0.0001
Combined uncertainty		0.0449

the imaginary refractive index of Eyjafjallajökull ash to be 0.000850 ± 0.00069 at 650 nm. The propagated uncertainty was then calculated according to Eq. (24). As can be seen in Fig. 6 and Table 2 the forward model sensitivity to k_p is small.

The modelling error associated with assuming spherical particles (and therefore Mie scattering) was estimated. T-matrix scattering code, described in [34] Mishchenko *et al.*, was used to calculate the configurationally averaged scattering amplitude functions, S_1 and S_2, for randomly orientated spheroids with an aspect ratio of 1.5 — an average aspect ratio of 1.47 ± 0.30 for Eyjafjallajökull ash was found in [22]. The forward model result using these non-spherical scattering amplitude functions was subtracted from the forward model result using Mie scattering amplitude functions to give $\Delta\mathbf{f}$. The gain matrix was then applied to compute the propagated uncertainty, according to Eq. (25).

5. Results

5.1. *Monodisperse polystyrene latex spheres*

The monodisperse CSM was used within a least squares retrieval weighted by measurement errors — see Eq. (22) — to retrieve the state vector $\mathbf{x} = \left(n_\mathrm{p}, n_\mathrm{m}\right)$ from the experimental reflectivity scans on the suspensions of polystyrene latex particles with varying volume filling

#247358 Received 5 Aug 2015; revised 27 Oct 2015; accepted 4 Nov 2015; published 25 Jan 2016

fractions in distilled water. The refractive index of the suspension medium n_m was retrieved because of the additional polymer dispersant present, which is likely to alter slightly the refractive index of the distilled water used to suspend the polystryrene particles. The volume filling fraction for each scan was fixed at its measured value in the retrieval. The vector of assumed model parameters had the form $\mathbf{b} = (f, a, \lambda)$, with the particle radius fixed at $a = 260$ nm and the incidence wavelength fixed at $\lambda = 635$ nm.

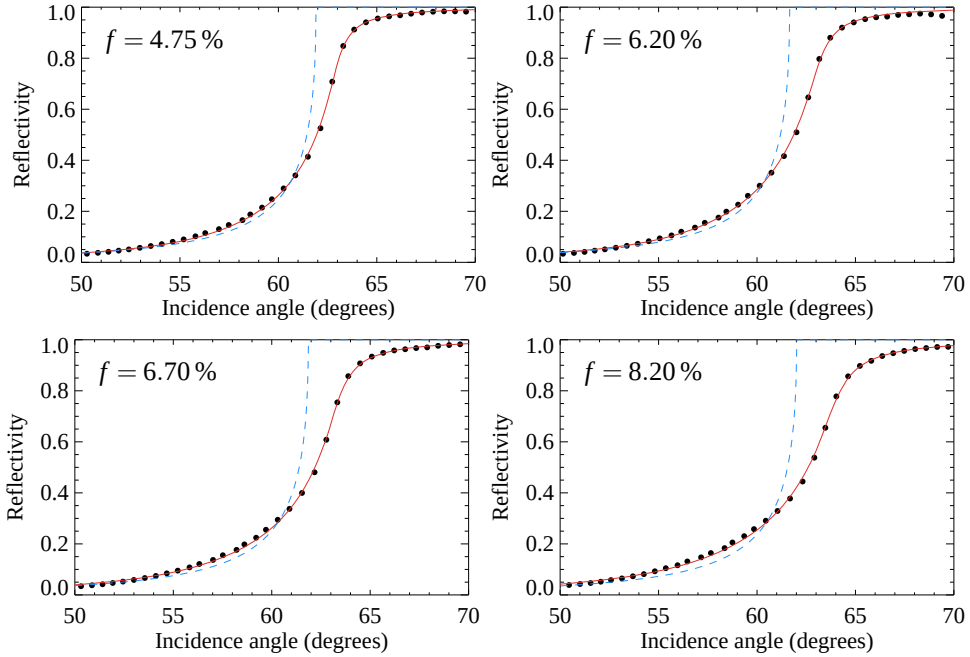

Fig. 7. Reflectivity scans for polystyrene latex spheres in distilled water at differing volume filling fractions. Shown are the fitted reflectivity curve —— using the monodisperse CSM and the Fresnel reflectivity curve - - - for a suspension medium containing no scatterers with a refractive index equal to the retrieved value of n_m.

Figure 7 shows the experimental data points at different volume filling fractions. The fitted reflectivity curves are shown in red. The Fresnel reflectivity for a homogeneous medium (containing no scatterers) with a refractive index equal to the retrieved value of n_m is shown as a dashed blue line.

Table 3 summarises the retrieval results for the polystryrene latex sphere suspensions of varying volume filling fraction. The weighted mean refractive index from the polystryrene scans is $< n_p >= 1.5931 \pm 0.0052$ at 635 nm. This compares to the value for the refractive index of polystyrene of 1.5870 ± 0.001 at 635 nm according to [41], Kasarova *et al*.

5.2. Polydisperse sand sample

The number of slabs, N, used to model the transition region was determined by analysing reflectivity curves, produced by the forward model, increasing N in increments of 5 (with all other parameters fixed). It was found that the reflectivity curves rapidly converged. The improvement in increasing the number of slabs beyond 50 was small; the maximum difference in reflectivity for $N = 50$ compared to $N = 100$ was less than 0.1 % (i.e. less than 10 % of the laser power uncertainty).

The polydisperse CSM using a 50 slab system to model the interface region was employed in

#247358 Received 5 Aug 2015; revised 27 Oct 2015; accepted 4 Nov 2015; published 25 Jan 2016

Table 3. Summary of polystyrene latex sphere retrieval results using the monodisperse CSM.

Measured f (%)	Retrieved n_{p}	Retrieved n_{m}
4.75	1.6045 ± 0.0127	1.3364
6.20	1.5932 ± 0.0120	1.3337
6.70	1.5933 ± 0.0117	1.3359
8.27	1.5868 ± 0.0111	1.3379
10.36	1.5906 ± 0.0109	1.3398

the retrievals. The particle size distribution was assumed to be log-normal. The median radius a_0 and width parameter S were retrieved. The state vector for the retrieval took the form $\mathbf{x} = \left(n_{\mathrm{p}}, n_{\mathrm{m}}, f, a_0, S\right)$ and the parameter vector was $\mathbf{b} = (\lambda)$. A least squares retrieval weighted by measurements errors was employed. The suspension medium refractive index was included as a retrieved parameter, as it is possible that the sand sample has a small component of soluble material which may alter slightly the refractive index of the distilled water used to suspend the sand.

Table 4. Summary of the retrieval results on the sand sample.

n_{p}	n_{m}	f (%)	a_0 (nm)	S
1.6099 ± 0.0586	1.3338	3.66	424.6	1.145
1.6211 ± 0.0553	1.3317	4.41	417.0	1.146
1.5837 ± 0.0449	1.3323	5.01	402.1	1.127
1.5603 ± 0.0446	1.3339	5.56	450.2	1.108
1.5530 ± 0.0551	1.3353	6.06	432.8	1.183
1.5370 ± 0.0548	1.3310	6.08	435.7	1.184

Table 4 summarises the retrieval results for the sand sample. The mean refractive index for the sand from the 6 scans is $< n_{\mathrm{p}} >= 1.576 \pm 0.021$ at 635 nm. This compares to values measured using the Becke line technique of 1.566 ± 0.01 at 546.1 nm and 1.560 ± 0.01 at 650 nm.

5.3. Polydisperse volcanic ash sample

The same type of retrieval, outlined in section 5.2, was used for the volcanic ash reflectivity data. As with the sand retrievals, the suspension medium refractive index was included as a retrieved parameter because the volcanic ash is likely to have a small soluble component that may alter slightly the refractive index of the distilled water used to suspend the ash.

Table 5 summarises the retrieval results for the volcanic ash samples. Sample A and sample B were produced from the same bulk ash sample, but were left to settle for 12 hours and 24 hours respectively for the sedimentation process. Table 5 shows a clear variation in the retrieved log-normal size distribution parameters between the two samples.

The mean refractive index from the 6 scans on volcanic ash was $< n_{\mathrm{p}} >= 1.553 \pm 0.024$ at 635 nm. The same volcanic ash sample's refractive index was measured using the Becke line method and was found to be 1.546 ± 0.01 at 546.1 nm and 1.548 ± 0.01 at 650 nm. The Becke line method is only applicable to particles with a radius larger than approximately 500 nm, as determined by the resolvable limit of the optical microscope used for the technique. Comparison with the result obtained using the reflectance measurements, indicates no evidence of a

#247358 Received 5 Aug 2015; revised 27 Oct 2015; accepted 4 Nov 2015; published 25 Jan 2016

Table 5. Summary of the retrieval results on samples made from an Icelandic volcanic ash. Sample A underwent a 12 hour sedimentation process whilst for Sample B the period was 24 hours.

Sample	n_p	n_m	f (%)	a_0 (nm)	S
A	1.5684 ± 0.0710	1.3346	3.18	314.5	1.278
A	1.5597 ± 0.0523	1.3345	8.23	314.1	1.285
A	1.5269 ± 0.0549	1.3358	9.19	323.8	1.313
B	1.5561 ± 0.0573	1.3334	5.97	208.2	1.503
B	1.5535 ± 0.0596	1.3369	9.48	241.6	1.426
B	1.5308 ± 0.0587	1.3366	10.66	255.1	1.411

variation in refractive index between the Becke line size regime and the size regime of the reflectance measurements (indicated by the retrieved modal radii in Table 5).

6. Conclusions

This paper determines the accuracy in retrieving the real refractive index, at visible wavelengths, of submicron monodisperse or polydisperse aerosol particles from angular reflectivity measurements of a dilute colloidal suspension of the aerosol. The coherent scattering model [26] has been applied to model the reflectivity from the colloidal suspension. An extension of this model for polydisperse suspensions, similar to that in [33], is presented which properly accounts for the modified particle size distribution close to the medium-to-colloid interface. The modified distribution occurs because a particle of radius a cannot approach closer than a to the interface, resulting in an increase in the relative density of smaller particles as the interface is approached. A sensitivity analysis was performed on the monodisperse and polydisperse models, which determines how experimental uncertainties propagate into uncertainty associated with the retrieval of real refractive index.

Experimental reflectivity data, at a wavelength of 635 nm, were obtained for a monodisperse suspension of polystryrene latex spheres with a known refractive index, a polydisperse sand sample and a polydisperse sample of volcanic ash. The monodisperse CSM was used to retrieve the real refractive index of the polystyrene particles, and the value obtained agreed with the known value to within uncertainties predicted by the sensitivity analysis. Similarly, the polydisperse CSM, using a 50 slab interface transition region and assuming a lognormal size distribution, was used to retrieve the real refractive index from the reflectivity data obtained for the sand and ash samples. The retrieved refractive index for the sand and ash samples agreed, to within derived uncertainties, with values obtained using the Becke line method on the same samples. However, comparison of refractive indices obtained from the two techniques is complicated because they are sensitive to different particle size regimes. The advantage of the technique, presented in this paper, is its sensitivity to submicron particles (as demonstrated by the sensitivity analysis of section 4, and in particular Fig. 6(b)) whereas the Becke line technique is limited by the resolving ability of an optical microscope, typically to particles with a diameter $> 1\,\mu$m.

In the forward model used to predict the reflectivity from the colloidal suspensions, spherical particles were assumed and therefore the Mie scattering amplitude functions used. However, volcanic ash particles are known to have irregular non-spherical shapes [23]. In principle, there is no reason why non-spherical scattering amplitude functions could not be used in the forward model replacing the assumed Mie scattering amplitude functions. By employing T-matrix code, we have included in the sensitivity analysis an estimate of the systematic uncertainty introduced

#247358 Received 5 Aug 2015; revised 27 Oct 2015; accepted 4 Nov 2015; published 25 Jan 2016

into the retrieval of real refractive index resulting from non-spherical scattering effects.

An area for possible improvement for retrieving the real refractive index of ash samples from this method would be to incorporate independent sizing measurements of the aerosol. In the retrievals performed on the reflectivity data from the polydisperse sand and ash samples, a lognormal distribution was assumed with a_0 and S being retrieved parameters. If accurate independent sizing data could be obtained for the submicron aerosol, their incorporation could significantly reduce uncertainties associated with the retrieval of real refractive index for polydisperse samples.

In conclusion we present a method for retrieving the real refractive index of submicron aerosol particles from near critical angle reflectivity measurements from a dilute colloid containing the aerosol. The technique has been successfully applied to monodisperse polystryrene latex spheres of radius 260 nm, a polydisperse sand sample and a polydisperse volcanic ash sample. In the future we aim to apply the method to a range of volcanic ash samples. Comparison of these results with those obtained using the Becke line method will allow any variation in real refractive index between submicron and particles larger than one micron to be investigated.

Acknowledgments

R.G.G. and D.M.P. acknowledge funding from the NERC VANAHEIM project NE/1015592/1 and the NERC SHIVA project NE/J023310/1. B.E.R. was funded by a NERC studentship NE/J500045/1. This study was funded as part of NERCs support of the National Centre for Earth Observation and the Centre for Observation and Modelling of Earthquakes, Volcanoes, and Tectonics.

#247358 Received 5 Aug 2015; revised 27 Oct 2015; accepted 4 Nov 2015; published 25 Jan 2016